

Article

Optoelectronic Properties of Hydrogen-Terminated Silicon Nanowires via Aliphatic C₈ Moieties: Impact of C–C Bond Order from First Principles

Francesco Buonocore ^{1,*}, Barbara Ferrucci ^{2,*}, Sara Marchio ¹, Simone Giusepponi ¹, Sumesh Sadhujan ³,
Musa Abu-Hilu ³, Muhammad Y. Bashouti ³ and Massimo Celino ¹

- ¹ Energy Technologies and Renewable Sources Department, Italian National Agency for New Technologies, Energy and Sustainable Economic Development (ENEA), Casaccia Research Centre, Via Anguillarese 301, 00123 Rome, Italy; sara.marchio@enea.it (S.M.); simone.giusepponi@enea.it (S.G.); massimo.celino@enea.it (M.C.)
- ² Fusion and Technology for Nuclear Safety and Security Department, Italian National Agency for New Technologies, Energy and Sustainable Economic Development (ENEA), Bologna Research Centre, Via dei Mille 21, 40121 Bologna, Italy
- ³ Department of Solar Energy and Environmental Physics, Swiss Institute for Dryland Environmental and Energy Research, J. Blaustein Institutes for Desert Research, Ben-Gurion University of the Negev, Midreshet Ben-Gurion, Building 26, Be'er Sheva 8499000, Israel; sadhujan@post.bgu.ac.il (S.S.); musa.abuhilu@gmail.com (M.A.-H.); bashouti@bgu.ac.il (M.Y.B.)
- * Correspondence: francesco.buonocore@enea.it (F.B.); barbara.ferrucci@enea.it (B.F.)

Abstract

In the present work we investigate by first principles calculations the structural, electronic, and optical properties of alkyl, 1-alkenyl and 1-alkynyl C₈ moieties chemisorbed on hydrogen-terminated silicon nanowire oriented along the <112> direction. Our results disclose how the nature of the carbon–carbon bond contiguous to the Si surface influences the behavior of the system. While 1-alkynyl groups exhibit the strongest Si–C bonding, it is 1-alkenyl functionalization that induces the most significant enhancement in optical absorption within the visible range due to charge transfer. The charge transferred from the nanowire to the moiety confirms the electronic coupling of the two systems. We found that the highest occupied molecular orbital of the 1-alkenyl moiety lies only 0.3 eV below the valence band edge of the hydrogen-terminated silicon nanowire, enabling new low-energy optical transitions which are absent in both the unmodified silicon nanowire and the isolated molecule. These findings demonstrate a synergistic effect of functionalization. Our study provides valuable insights into the design of functionalized silicon nanostructures with tailored optical properties, with potential implications for applications in sensing, photonics, and energy conversion.

Keywords: silicon nanowires; Surface functionalization; optoelectronic properties; density functional theory



Academic Editor: Andrea Li Bassi

Received: 24 July 2025

Revised: 10 September 2025

Accepted: 16 September 2025

Published: 19 September 2025

Citation: Buonocore, F.; Ferrucci, B.; Marchio, S.; Giusepponi, S.; Sadhujan, S.; Abu-Hilu, M.; Bashouti, M.Y.; Celino, M.

Optoelectronic Properties of Hydrogen-Terminated Silicon Nanowires via Aliphatic C₈ Moieties: Impact of C–C Bond Order from First Principles. *Appl. Sci.* **2025**, *15*, 10235. <https://doi.org/10.3390/app151810235>

Copyright: © 2025 by the authors. Licensee MDPI, Basel, Switzerland. This article is an open access article distributed under the terms and conditions of the Creative Commons Attribution (CC BY) license (<https://creativecommons.org/licenses/by/4.0/>).

1. Introduction

The continuous drive toward miniaturization and enhanced performance in modern technologies has brought low-dimensional systems to the forefront of materials research. Among these, silicon nanowires (SiNWs) have emerged as particularly promising nanostructures due to their unique physical and chemical properties, which differ significantly from their bulk counterparts. These one-dimensional systems are being intensively investigated for their potential in a broad spectrum of applications, including nanoelectronics [1–4], energy [5–10], and chemical and biochemical sensing [11–14].

A defining characteristic of SiNWs is their high surface-to-volume ratio, a consequence of their sub-100 nm diameters. This high surface sensitivity makes SiNWs exceptionally responsive to chemical surface processes, through which their surface potential and charge distribution can be effectively modulated [4,15–17].

Moreover, SiNWs have also been proposed as model systems for porous silicon, as suggested in early studies exploring carrier localization and photoluminescence phenomena [18].

In many device architectures, native oxide layer on SiNW surfaces, formed almost instantaneously upon exposure to air, introduces interface states within the silicon band gap, which can significantly lower device performance [19,20]. To mitigate this issue, it is essential to protect SiNW surfaces from oxidation. One common approach involves hydrogen termination, where surface-bound hydrogen atoms (Si–H) passivate dangling bonds, resulting in an oxide-free shell. However, these H-terminated surfaces are highly reactive and prone to rapid oxidation upon exposure to ambient conditions, leading to increased surface recombination velocities and reduced carrier lifetimes [21,22].

To ensure long-term stability and preserve low surface recombination rates, more robust surface passivation strategies are required. Covalent attachment of organic molecules to the silicon surface via Si–C bonds has been shown to offer superior resistance to oxidation and lower electron-hole recombination rates compared to H-terminated surfaces [14,23].

In a different context, a key objective in the design of silicon nanowire (SiNW)-based devices is the precise control of interface energetics through surface functionalization, achieved by immobilizing organic molecules on SiNWs [23–27]. This strategy is particularly relevant for applications in electronics, photovoltaics, and biosensing. Organic monolayers can introduce a net electrical dipole-oriented perpendicular to the surface/interface [14,28,29], thereby modifying the work function and electron affinity. As a result, the band offset and band bending at the interface can be tuned, enabling control over charge transfer processes. Such band alignment engineering is crucial for optimizing charge transfer in energy-related devices, including batteries and energy storage systems [30,31]. Furthermore, understanding the impact of molecular functionalization on the optoelectronic properties of SiNWs is particularly relevant when considering their application in photovoltaic devices [32,33].

In our previous work, we investigated dipole formation on hydrogen-terminated silicon surfaces functionalized with aliphatic molecules, and its impact on Schottky and tunneling barriers [34]. Prior to that, we studied the adsorption of octane moieties on the (111) and (110) facets of fully H-passivated SiNWs (SiNW:H) [35]. However, the latter study was limited by a narrow exploration of initial adsorption configurations and by the exclusive focus on alkyl chains, where only C–C single bonds were present near the surface.

To advance this understanding, it is essential to explore the effects of chemisorption of 1-alkenyl and 1-alkynyl moieties on SiNW, which introduce C=C double and C≡C triple bonds, respectively, in proximity to the surface. These unsaturated bonds are expected to significantly influence the electronic and optical properties of SiNWs. Therefore, in the present study, we employ *ab initio* calculations to compare the adsorption energetics of alkyl, 1-alkenyl, and 1-alkynyl C₈ moieties on SiNW:H oriented along the ⟨112⟩ direction, and then we explore how the optical properties are modified by SiNW functionalization. Our goal is to identify the most suitable functionalization strategy depending on the desired electronic and optical properties.

2. Methods

In order to study the structural, electronic and optical properties of the aliphatic C₈ moieties on SiNW:H, a first principles approach based on the periodic density functional theory (DFT) [36,37] was adopted. All the total energy calculations were performed using

the PWSCF (plane-wave self-consistent field) code of the Quantum ESPRESSO [38,39] that performs different kinds of self-consistent calculations of electronic-structure properties. Quantum ESPRESSO is an integrated suite of computer codes for electronic-structure calculations and materials modeling at the nanoscale. The Perdew–Burke–Ernzerhof (PBE) functional [40] in the generalized gradient approximation (GGA) was used to treat the exchange-correlation energies while the ultrasoft pseudopotentials in Vanderbilt implementation [41] were adopted to model the electron-ion interactions. Preliminary self-consistent calculations on the total energy (E_T) were performed on the pseudopotential to set the cut-offs and the k-points grid. The kinetic energy cut-off was set to 30 Ry to expand on a plane-wave basis set the electronic wave functions, while the charge density cut-off was set ten times greater (300 Ry). A k-point mesh of $4 \times 1 \times 1$ Monkhorst-Pack [42] with no shift was used to sample the Brillouin zone. Moreover, to account for van der Waals interactions, the DFT-D3 parametrization of density functional dispersion [43] was employed. The geometric structures were fully relaxed and optimized by setting the conditions that the energy change between two consecutive self-consistent field steps was less than 10^{-4} Ry, and the minimal force acting on an atom became less than 10^{-3} Ry/Bohr.

Löwdin analysis was used to quantitatively estimate the charge transfer between the SiNW:H and the chemisorbed alkyl, 1-alkenyl and 1-alkynyl C_8 moieties. The non-self-consistent calculation of the electronic states is performed on a $48 \times 1 \times 1$ k-points grid, which was found to yield an accurate representation of the density of states.

Optical properties have been calculated within the single particle approach using the Fermi golden rule that involves the computation of the transition matrix elements of the momentum operator. The longitudinal optical conductivity σ_x has been derived from the imaginary part of the dielectric function ϵ_x component along longitudinal direction of the SiNW using the same methodology illustrated in [44] as follows:

$$Re(\sigma_x) = \frac{\omega \cdot S \cdot Im(\epsilon_x)}{4\pi} \quad (1)$$

where S is the cross-section of the supercell, $\hbar\omega$ is the photon energy and \hbar is the reduced Planck constant. In the calculations σ_x has been normalized to quantum conductivity $\sigma_0 = \frac{e^2}{4\hbar}$, where e is the electron charge, and the lattice period of the SiNW along the longitudinal direction L . For example, a normalized longitudinal optical conductivity value of 1 corresponds to a bulk optical conductivity σ_{bulk} of 3.7×10^3 S/m.

The mesh of k-points $96 \times 1 \times 1$ has been chosen to guarantee well converged optical spectra. The real part of the optical conductivity provides direct insight into the optical absorption characteristics of the system. It quantifies the material's ability to absorb electromagnetic radiation at different photon energies. Peaks in the real part of the optical conductivity spectrum correspond to allowed electronic transitions between occupied and unoccupied states, and their intensity reflects the strength of these transitions. Therefore, analyzing this quantity allows us to identify the energy ranges where the system is optically active and to assess how different surface functionalization modifies the absorption profile of the SiNW.

Based on our previous investigations [35], we adopt the model for the SiNW:H oriented along the $\langle 112 \rangle$ direction with diameter of 1.7 nm, consisting of 192 atoms of Si, and 79 atoms of H. Indeed, in our previous study [35] we found that for this diameter the effects of the high ratio of H/Si number of atoms in the smaller SiNW (i.e., H states close to the valence band edge) are not observed. The cross-section of the SiNW:H is shown in Figure 1, along with side views of the Si(111) and Si(110) exposed facets. The supercell used for the adsorption cases is built by replicating twice along the longitudinal direction the cell of the SiNW. A vacuum gap of at least 20 Å in the cross-section plane has been introduced to

exclude interaction among supercell replicas by adopting an orthorhombic supercell with lattice parameters $a = 13.69 \text{ \AA}$ ($L = a$), $b = 45.47 \text{ \AA}$ and $c = 48.94 \text{ \AA}$.

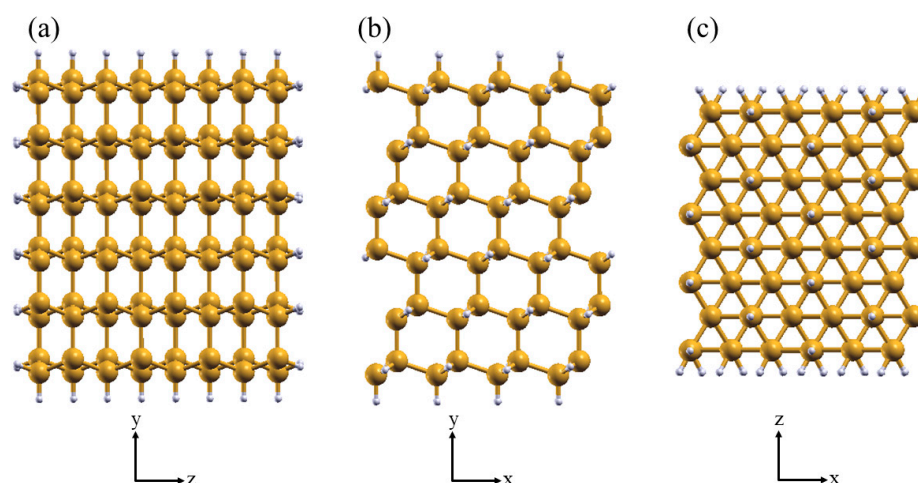


Figure 1. (a) Top view of SiNW cross-section. (b,c) Side view of the exposed (110) and (111) facets, respectively (yellow and white spheres are Si and H atoms, respectively).

3. Results

In the following we investigate the geometrical structure as well as the electronic and optical properties of alkyl, 1-alkenyl, and 1-alkynyl C_8 moieties chemisorbed on SiNW oriented along the $\langle 112 \rangle$ direction.

3.1. Structural Properties of Aliphatic Moieties Chemisorbed on SiNW:H

We screened a wide range of possible adhesion configurations of molecules with single, double, and triple carbon–carbon bonds attached to the H–Si(111) and H–Si(110) surface and performed the structural optimization of each of them [45]. In the present work, we focused on C_8 moieties and used as starting configuration the adsorption geometry corresponding to the minimal energy of adhesion on the corresponding planar surface, then we relaxed the geometry. This second optimization of the functionalized NWs introduced only minor changes with respect to the initial molecular orientation.

The six systems, consisting of alkyl, 1-alkenyl, and 1-alkynyl C_8 moieties chemisorbed on (111) and (110) SiNW facets, are shown in Figure 2a–c,e–g, respectively. For each of them, we estimated the molecular tilt angle $\theta(C_1C_8)$ by evaluating the angle between the surface normal and the vector connecting atoms C_1 and C_8 . Similarly, we calculated the orientation of the C_1 – C_2 bond with respect to the surface normal, $\theta(C_1C_2)$. Both $\theta(C_1C_8)$ and $\theta(C_1C_2)$ are schematically illustrated in Figure 2d. The corresponding values are listed in Table 1, along with the distance of the C_1 – C_2 and Si– C_1 bonds, evaluated for each system. The azimuthal rotation of the moieties has a minor influence on the results and is therefore omitted here for the sake of simplicity. For the alkyl moiety, the most stable configurations correspond to a tilt angle $\theta(C_1C_8)$ of 36° on the (111) surface and 4° on the (110) surface, with $\theta(C_1C_2)$ measuring 61° and 33° , respectively. For the 1-alkenyl moiety, $\theta(C_1C_8)$ is approximately 35° on both surfaces, while $\theta(C_1C_2)$ is equal to 55° on the (111) surface and 48° on the (110) surface. The 1-alkynyl moiety exhibits a larger tilt angle in its stable configurations compared to the other two groups, with $\theta(C_1C_8)$ equal to 66° on the (111) surface and 56° on the (110) surface, and $\theta(C_1C_2)$ corresponding to 22° and 29° , respectively. The larger tilt angle of the 1-alkynyl group can be associated with the rigidity of the σ bond and the two π bonds forming the triple bond. The tilting angle of the moiety impacts the surface dipole, that in this way depends on C bonds hybridization. The C_1C_2 bond length varies according to the C–C bond order in the molecule. For the

single (alkyl), double (1-alkenyl) and triple (1-alkynyl) C-C bond, the distance $d(C_1C_2)$ was found to be approximately 1.53 Å, 1.36 Å, and 1.23 Å, respectively. The Si-C₁ bond length (the first carbon bonded to silicon) $d(C_1Si)$ also decreases with increasing bond order, with values of 1.91 Å for C₈ alkyl, 1.86 Å for C₈ 1-alkenyl, and 1.82 Å for C₈ 1-alkynyl.

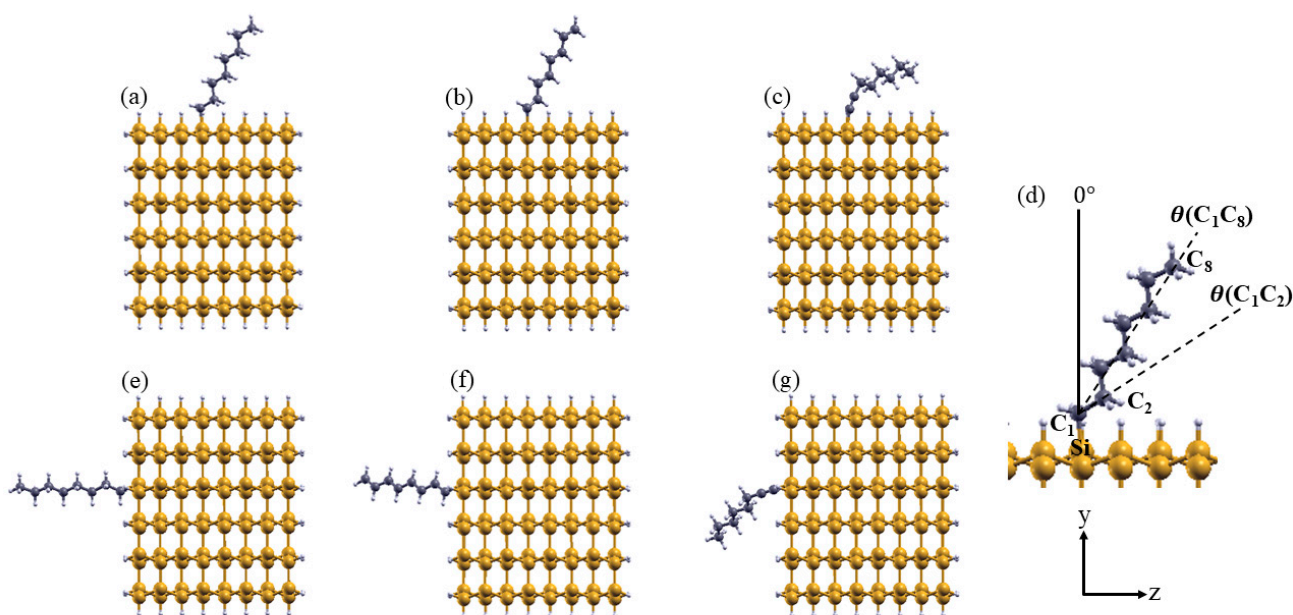


Figure 2. Top view of the SiNW functionalized with alkyl (a,e), 1-alkenyl (b,f), and 1-alkynyl (c,g) C₈ moieties grafted onto SiNW:H (111) (a-c) and SiNW:H (110) (e,f). (d) Schematic representation of the geometrical parameters ($\theta(C_1C_8)$, $\theta(C_1C_2)$, $d(C_1C_2)$, $d(C_1Si)$) used in the analysis (yellow, white and gray spheres are Si, H and C atoms, respectively).

The variation in the C₁C₂ and SiC₁ bond distances for the three molecules is due to the hybridization of the C₁ atom. As it changes from sp³ to sp² to sp, the orbitals become more localized, leading to shorter bonds and increased bond strength. The obtained values agree with standard bond lengths [46,47].

The bond dissociation energy (BDE) of the modeled systems is calculated using the formula [48]:

$$BDE = E_{H-SiNW} + E_{moiety} - E_T \quad (2)$$

where E_T is the total energy of the full system and E_{H-SiNW} and E_{moiety} are the total energies of the relaxed H-SiWNs missing one H atom in the binding site and the aliphatic moiety, respectively. In Equation (2), we omitted to take into account the vibrational Helmholtz free energy that should be evaluated by phonon calculations under the quasi-harmonic approximation. This is beyond the scope of the present paper since the accurate estimation of the vibrational free energy would require a careful study of the phonon dispersion for the large structures examined. This makes it impractical to include calculations of the vibrational modes in our stability study. However, typical zero-point energy (ZPE) corrections are on the order of tens of meV (1–5 kJ/mol) per molecule [49], lower than the BDE differences we calculated. Moreover, ZPE corrections should be of similar sign and magnitude for the three types of C₈ moieties investigated, preserving the trend in BDE.

The BDE values reported in Table 1 reveal a clear trend in the stability of the surface functionalized SiNW:H. Among the three C₈ moieties investigated, the 1-alkynyl group exhibits the highest BDE, followed by the 1-alkenyl group, while the 1-alkyl chain shows the lowest BDE. This trend is reproduced across both the (111) and (110) surface orientations. Notably, we found a systematic rise in binding strength of about 100 kJ/mol with increasing bond order of the carbon moiety near the surface, from single (alkyl) to double (1-alkenyl) to

triple (1-alkynyl) bonds. Such a trend underlines the importance of π -bonding interactions in enhancing the stability of the Si–C interface.

Table 1. Geometric parameters and bond dissociation energy of the aliphatic C₈ moieties chemisorbed on SiNW:H (111) and (110) facets. Refer to Figure 2 for the meaning of the listed parameters and atomic labels of the modeled systems. Bond lengths are in Ångstrom, angles are in degrees and energies are in kJ/mol.

NW Structure	$\theta(\text{C}_1\text{C}_8)$	$\theta(\text{C}_1\text{C}_2)$	$d(\text{C}_1\text{C}_2)$	$d(\text{C}_1\text{Si})$	BDE
alkyl-SiNW:H (111)	36.43	60.87	1.53	1.91	602.82
1-alkenyl-SiNW:H (111)	35.19	55.13	1.36	1.87	712.99
1-alkynyl-SiNW:H (111)	66.50	22.34	1.23	1.82	814.55
alkyl-SiNW:H (110)	3.54	32.77	1.53	1.91	600.08
1-alkenyl-SiNW:H (110)	34.84	47.78	1.36	1.86	712.00
1-alkynyl-SiNW:H (110)	56.12	28.55	1.23	1.82	820.83

3.2. Electronic Properties of Aliphatic Moieties Chemisorbed on SiNW:H

To investigate the electronic structure of SiNW:H functionalized with different C₈ moieties, we analyzed the Projected Density of States (PDOS) for each system (Figure 3). Our results indicate that the PDOS is only weakly dependent on the surface orientation; thus, for clarity, we present representative PDOS plots for each moiety chemisorbed on the (111) surface. In all plots, the valence band maximum (VBM) is aligned to 0 eV.

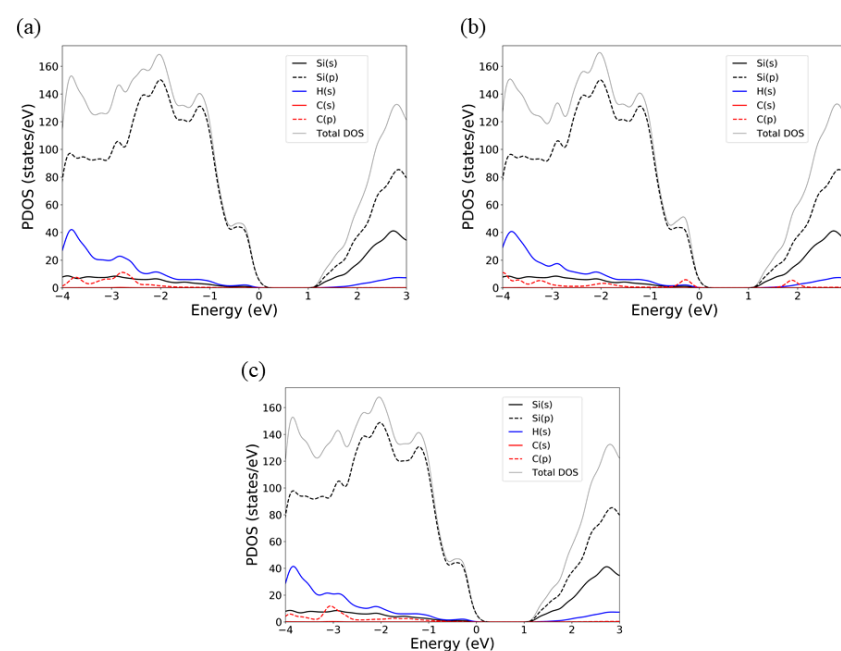


Figure 3. Projected electron density of states (PDOS) of aliphatic C₈ moieties: (a) alkyl-SiNW:H; (b) 1-alkenyl-SiNW:H; (c) 1-alkynyl-SiNW:H systems.

The SiNW:H exhibits a calculated band gap of approximately 1.3 eV, which remains largely unchanged upon chemisorption of any of the three C₈ moieties. The energy gap of SiNW is enlarged with respect to the calculated PBE energy gap of bulk silicon due to quantum confinement effects. The bandgap of 1.3 eV calculated using the PBE functional for a 1.7 nm SiNW is significantly lower than experimental [50] and GW calculated values, [51] which range from 2.2 to 2.8 eV. The same calculated bandgap of bulk silicon using the PBE functional is 0.61 eV, which is significantly lower than the experimental value of 1.12 eV. These discrepancies are known limitation of semi-local DFT functionals such as PBE, which

tend to underestimate bandgaps. Despite this, PBE remains reliable for analyzing relative trends across similar systems.

It is important to observe that none of the functional groups introduce mid-gap states, indicating that the SiNW remains passivated. The 1-alkyl moiety contributes occupied states located approximately 2 eV below the VBM, while the 1-alkynyl moiety exhibits a similar behavior, with occupied states beginning around 1 eV below the VBM. The values of the highest occupied molecular orbital (HOMO) and the lowest unoccupied molecular orbital (LUMO) energy levels, as well as the HOMO-LUMO gap of the moieties adsorbed to SiNW:H are reported in Table 2 (see also Supplementary Materials).

Table 2. HOMO and LUMO energy levels, and HOMO-LUMO gaps of the moieties adsorbed to SiNW:H (units are eV).

Moiety	HOMO	LUMO	HOMO-LUMO Gap
alkyl C ₈	−2.75	2.70	5.45
1-alkenyl C ₈	−0.30	1.90	2.20
1-alkynyl C ₈	−1.45	3.10	4.45

The valence band is mainly composed of silicon p-orbitals (Si(p)), while the conduction band shows contributions from both silicon s- and p-orbitals, with Si(p) still being dominant. It is worth noting that the 1-alkenyl-functionalized system exhibits a distinct feature: its frontier molecular orbitals lie relatively close to the SiNW band edges. Specifically, the HOMO is located just 0.3 eV below the VBM, and LUMO lies 0.6 eV above the conduction band minimum (CBM), or equivalently, 1.9 eV above the VBM (Table 2).

This contiguity of the frontier orbitals to the band edges has important implications. Indeed, the presence of HOMO levels near the valence band edge suggests that charge can be accumulated close to the surface. On the other side, it may enhance the optical activity of the functionalized SiNW due to charge transfer. Charge transfer and optical absorption will be explored in the subsequent sections.

3.3. Charge Transfer of Aliphatic Moieties Chemisorbed on SiNW:H

To improve the understanding of the interaction between the SiNW:H facets and the chemisorbed aliphatic moieties, we analyzed both Löwdin charges and charge density difference isosurfaces. The calculated charge transfer from the substrate to the chemisorbed moiety reveals a clear trend: approximately 0.20 *e* for the alkyl group, 0.30 *e* for the 1-alkenyl group, and 0.35 *e* for the 1-alkynyl group. These values are consistent across both (111) and (110) SiNW facets, indicating that the nature of the chemisorbed moiety plays a more significant role than the surface orientation.

A general trend emerges: the amount of charge transferred increases with the bond order of the carbon–carbon bond closest to the surface. This is attributed to the increased electron localization associated with higher bond orders, as illustrated by the charge density difference plots in Figure 4 (see also Supplementary Materials). These plots show an accumulation of electronic charge along the Si–C bond and over the carbon atom directly bonded to silicon. Simultaneously, we observe charge depletion around the silicon atom and near the bond edge of the nearby carbon atom. Additional, though less pronounced, charge redistribution is also visible along the C–C bonds near the Si–C interface. In particular, the 1-alkynyl moiety exhibits a more substantial accumulation of negative charge around the triple bond closest to the surface.

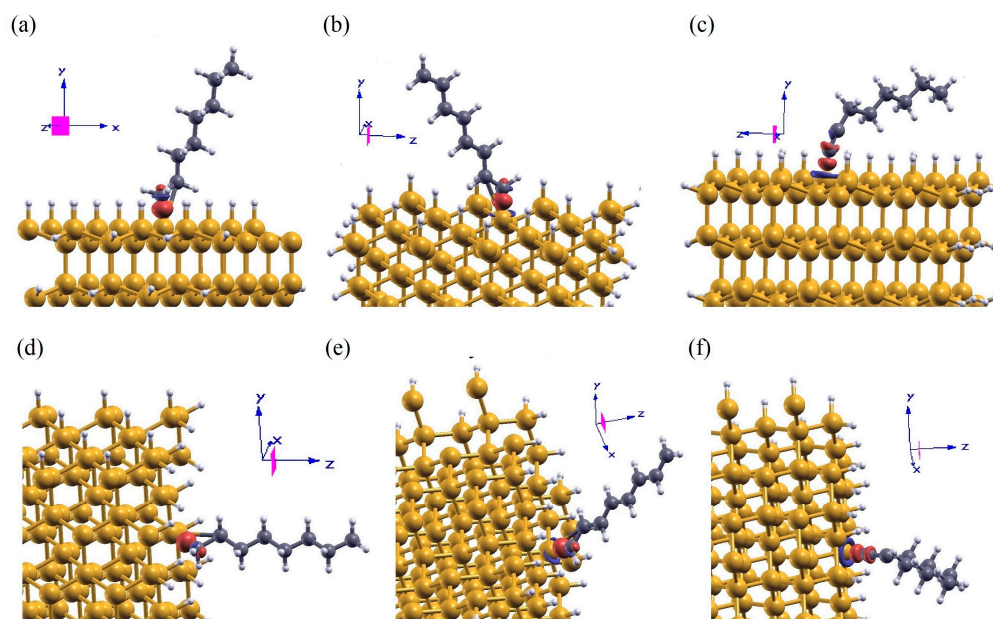


Figure 4. Difference in the charge density of alkyl (a,d), 1-alkenyl (b,e) and 1-alkynyl (c,f) C₈ moieties chemisorbed on SiNW:H (111) (a–c) and (110) (d–f) facet, respectively (yellow, white and gray spheres are Si, H and C atoms, respectively; red and blue are positive and negative isosurfaces, respectively; isosurface value is ± 0.005 a.u.).

3.4. Optical Properties of Aliphatic Moieties Chemisorbed on SiNW:H

To evaluate the impact of aliphatic functionalization on the optical activity of SiNW:H, we analyzed the longitudinal optical conductivity σ_x in the low-energy regime. Figure 5 presents the σ_x spectra for SiNW:H functionalized with the three C₈ moieties. Considering that the electronic structure is independent on the facet where moiety is chemisorbed, we present representative optical conductivity plots for each moiety chemisorbed on the (111) surface. The absorption onset, corresponding to the fundamental band gap transition of 1.3 eV of SiNW:H, is not visible in the Figure due to the scale adopted.

Among the three systems, the 1-alkenyl-functionalized SiNW:H exhibits the most pronounced optical response. The 1-alkenyl system shows a sharp increase in optical conductivity at 1.6 eV, followed by a wide peak in the 1.8–2.0 eV range, significantly stronger than that observed for the alkyl- and 1-alkynyl-functionalized SiNW:H. The analysis of the oscillator strengths allowed to discriminate that the electronic transition at 1.9 eV from the valence band to the fifth conduction band is the strongest electronic transitions contributing to the optical absorption in the 1.6–2.0 eV range. In contrast, both alkyl- and 1-alkynyl-functionalized SiNW:H display a sharp increase in optical response at around 1.8 eV, closely following the trend of the pristine SiNW:H. Even in the 2.0–2.3 eV range, where the 2.2 eV excitation corresponds to the HOMO–LUMO transition of the adsorbed moiety, the 1-alkenyl-functionalized system maintains higher optical conductivity. Beyond 2.4 eV, all three systems exhibit peaks of comparable intensity.

A particularly interesting feature of the 1-alkenyl-functionalized SiNW:H is the emergence of new optical transitions below the band gap of the isolated molecule calculated to be 2.4 eV. These transitions originate from the HOMO of the 1-alkenyl moiety to hybrid conduction states located below the LUMO, indicating a strong electronic coupling between the molecule and the substrate. This effect is absent in the alkyl and 1-alkynyl systems, whose HOMOs lie deeper within the valence band and are thus less optically active.

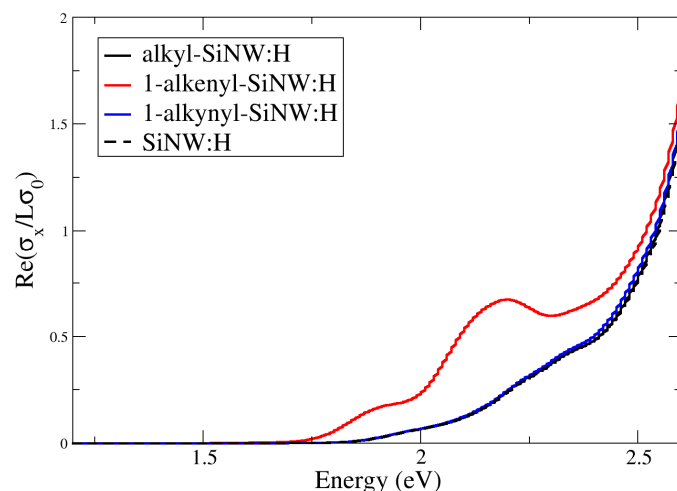


Figure 5. Real part of longitudinal optical conductivity σ_x of alkyl-, 1-alkenyl- and 1-alkynyl-SiNW:H in the low energy range. The σ_x of SiNW:H is reported as reference.

4. Discussion

Our investigation reveals that the enhanced low-energy optical absorption observed in SiNW:H upon functionalization with 1-alkenyl C_8 moieties is directly linked to the electronic alignment of the HOMO of the chemisorbed group. Specifically, the HOMO of the 1-alkenyl moiety lies only 0.3 eV below the VBM of the functionalized SiNW, enabling optical transitions near the band edge. In contrast, the HOMOs of the alkyl and 1-alkynyl moieties are located deeper within the valence band, resulting in significantly weaker optical activity in the same energy range.

Our analysis focused on the visible spectral window, which is particularly relevant for optoelectronic applications. We found optical transitions peculiar to the 1-alkenyl moiety functionalization in the energy range 1.6–2.4 eV. It is important to note, however, that the use of the PBE exchange–correlation functional is known to underestimate excitation energies due to its inherent limitations in describing quasiparticle states. While our results capture qualitative trends reliably, more accurate predictions of absolute transition energies would require the use of more computationally demanding methods. Despite the limitations of DFT calculations in predicting absolute values, such as band gaps, it remains a powerful tool for comparative studies. Indeed, when comparing similar systems, as in our case SiNWs functionalized with different carbon–carbon bond types, the systematic errors in PBE tend to cancel out, allowing reliable relative comparisons [52]. Moreover, PBE can capture qualitative changes in electronic structure due to variations in bonding. These changes influence the local density of states and charge distribution, which are central to understanding functionalization effects [26,53,54]. We observe that the HOMO–VBM offset for the 1-alkenyl moiety is reduced from 0.4 eV on planar Si(111) surface (as found in [34]) to 0.3 eV on the SiNW. This shift can be attributed to quantum confinement effects arising from the SiNW small diameter (1.7 nm), which modifies the electronic structure and enhances orbital overlap at the interface.

Charge transfer analysis further supports the interaction at the Si–C interface. Löwdin charge calculations and charge density difference isosurfaces indicate a net transfer of electronic charge from the SiNW to the chemisorbed moiety. This charge redistribution is determined by the coupling between moiety and nanowire and facilitates the emergence of new optical transitions in the energy range between the intrinsic SiNW band gap and the HOMO–LUMO energy gap of the isolated 1-alkenyl moiety. These transitions are attributed to excitations from the HOMO into hybridized conduction states of the SiNW. This behavior exemplifies a synergistic effect of functionalization, where the resulting optoelectronic

properties are not merely additive but arise from the formation of new transitions. The 1-alkenyl moiety chemisorption introduces enhanced optical features that are fundamentally different from those of the unmodified SiNW:H or the standalone molecule. While the effects of functionalization with carbon chain molecules on the stability of nanomaterials have been investigated in both experimental and theoretical studies [19,23,35,55,56], to the best of our knowledge, the impact of alkenyl moieties on optical absorption had not been reported prior to the present work.

Notably, density functional theory calculations have predicted that adsorption of certain organic molecules can significantly alter the optical spectra of silicon surfaces. For example, Molteni et al. [57] reported pronounced modifications in the optical properties of Si(001) upon eumelanin adsorption, highlighting the general impact that organic–semiconductor interfaces can have on optical behavior.

Moreover, there is experimental evidence that the adsorption of organic molecules can enhance the performance of hybrid silicon–based solar devices. In particular, He et al. demonstrated that the adsorption of small organic semiconductors on Si nanowires can lead to significant improvements in power conversion efficiency for hybrid heterojunction solar cells [58]. Similarly, Shen et al. found that modifying Si solar cells with conjugated polymers yields higher photovoltaic efficiency due to the introduction of new optical absorption pathways and improved interface quality [59].

These findings, taken together, underscore the pivotal role that organic functionalization, particularly with conjugated groups like alkenyls, can play in engineering the optoelectronic properties of silicon nanostructures, providing a promising route for modulating and enhancing their optical and photovoltaic properties.

These findings have broader implications for the design of functionalized silicon-based nanostructures. Pioneering studies [60] have long suggested a link between the optical properties of porous silicon and surface chemistry. Our results support and extend this view, indicating that targeted functionalization, especially with π -conjugated moieties like 1-alkenyl groups, can be a powerful strategy to engineer the optical response of nanostructured silicon. For example, high porosity silicon systems composed of nanometer scale columnar structures may benefit from such functionalization, enabling the emergence of novel optical functionalities relevant for sensing, photonics, and energy conversion applications.

5. Conclusions

In this work, we performed a systematic exploration of double/triple bond effects and direct *ab initio* connection to optical absorption and charge transfer, with earlier studies mainly focused on alkyl (single-bonded) groups or limited geometries. We compared single-, double-, and triple-bonded C₈ moieties on SiNW:H and addressed both energetics and optical consequences. DFT calculations revealed the emergence of new transitions only in the presence of 1-alkenyl moieties. As far as we know, this mechanism was not previously reported for SiNWs.

Our analysis of BDE revealed a clear trend: binding strength increases with the bond order of the chemisorbed moiety, with 1-alkynyl groups forming the most stable Si–C bonds. However, it is 1-alkenyl functionalization that introduces the most significant modifications to the optical properties of the SiNW:H. Indeed, the proximity of the 1-alkenyl HOMO to the valence band edge of the SiNW:H allows for the emergence of optical transitions from the HOMO into hybridized conduction states of the SiNW. Charge density difference and Löwdin charge analyses confirmed the coupling at the Si–C interface which in the case of the 1-alkenyl moiety facilitates charge transfer and enhances optical absorption in the visible range. These findings underscore a synergistic effect of functionalization.

Our results not only strengthen the understanding of molecule–nanowire interactions but also suggest a promising strategy for tailoring the optical response of silicon-based nanostructures through selective surface chemistry. These insights may be extended to other silicon nanostructures, including porous silicon, where functionalization with π -conjugated moieties such as alkenyl groups could unlock new functionalities for applications in sensing, photonics, and energy conversion.

Supplementary Materials: The following supporting information can be downloaded at: <https://www.mdpi.com/article/10.3390/app151810235/s1>. Figure S1: Plane averaged difference in the charge density; Figures S2 and S3: Schematic representations of energy levels; Figure S4: Longitudinal dielectric function; File S1: Atomic coordinates and Löwdin charge analysis.

Author Contributions: Conceptualization, F.B., B.F., S.S., M.A.-H. and M.Y.B.; Data curation, F.B., B.F. and S.M.; Formal analysis, F.B., S.M. and S.G.; Funding acquisition, M.C.; Investigation, F.B. and B.F.; Methodology, F.B., B.F., S.M. and S.G.; Project administration, M.C.; Resources, F.B.; Software, F.B., B.F. and S.G.; Supervision, F.B.; Validation, F.B., S.M., S.G. and M.C.; Visualization, F.B., B.F. and S.M.; Writing—original draft, F.B.; Writing—review and editing, F.B., B.F., S.M., S.G. and M.C. All authors have read and agreed to the published version of the manuscript.

Funding: This work was supported by the European Union through the Next Generation EU funds through the Italian MUR National Recovery and Resilience Plan, Mission 4 Component 2—Investment 1.4—National Center for HPC, Big Data and Quantum Computing—CUP I33C22001270007.

Data Availability Statement: Data available on request from the authors.

Acknowledgments: The computing resources and the related technical support used for this work have been provided by CRESCO/ENEAGRID High Performance Computing infrastructure and its staff [61]. CRESCO/ENEAGRID High Performance Computing infrastructure is funded by ENEA, the Italian National Agency for New Technologies, Energy and Sustainable Economic Development and by Italian and European research projects, see <http://www.cresco.enea.it/english> (accessed on 30 April 2025) for information. The authors acknowledge the extensive use of the ENEA FARO facility and the support of its management team [62]. M.B. thanks Sherina Harilal and Yihang Mao for useful discussions. F.B. thanks Olivia Pulci for useful discussions.

Conflicts of Interest: The authors declare no conflicts of interest.

Abbreviations

The following abbreviations are used in this manuscript:

BDE	Bond Dissociation Energy
HOMO	Highest Occupied Molecular Orbital
LUMO	Lowest Unoccupied Molecular Orbital
SiNW	Silicon NanoWire
SiNW:H	H-terminated Silicon NanoWire
DFT	Density Functional Theory
PBE	Perdew, Burke and Enzerholf exchange-correlation
GGA	Generalized Gradient Approximation
PDOS	Projected Density of States
VBM	Valence Band Maximum
CBM	Conduction Band Minimum
ZPE	Zero-Point Energy

References

1. Long, Y.-Z.; Yu, M.; Sun, B.; Gu, C.-Z.; Fan, Z. Recent Advances in Large-Scale Assembly of Semiconducting Inorganic Nanowires and Nanofibers for Electronics, Sensors and Photovoltaics. *Chem. Soc. Rev.* **2012**, *41*, 4560. [CrossRef]
2. Zhou, W.; Dai, X.; Fu, T.-M.; Xie, C.; Liu, J.; Lieber, C.M. Long Term Stability of Nanowire Nanoelectronics in Physiological Environments. *Nano Lett.* **2014**, *14*, 1614–1619. [CrossRef]

3. Shalabny, A.; Buonocore, F.; Celino, M.; Shalev, G.; Zhang, L.; Wu, W.; Li, P.; Arbiol, J.; Bashouti, M.Y. Semiconductivity Transition in Silicon Nanowires by Hole Transport Layer. *Nano Lett.* **2020**, *20*, 8369–8374. [[CrossRef](#)]
4. Laajimi, R.; Laajimi, K.; Rahmani, M. High-Precision Machine Learning Analysis of Photoluminescence and I-V Measurements in SiNWs-Based Schottky Diodes. *J. Lumin.* **2025**, *286*, 121379. [[CrossRef](#)]
5. Puglisi, R.A.; Di Franco, S.; La Magna, A.; Buongiorno, C.; Garozzo, C. Mannino Giovanni Molecular Doping Applied to Si Nanowires Array Based Solar Cells. *Sol. Energy Mater. Sol. Cells* **2014**, *132*, 118–122. [[CrossRef](#)]
6. Sahoo, M.K.; Kale, P. Integration of Silicon Nanowires in Solar Cell Structure for Efficiency Enhancement: A Review. *J. Mater.* **2019**, *5*, 34–48. [[CrossRef](#)]
7. Yang, Y.; Yuan, W.; Kang, W.; Ye, Y.; Pan, Q.; Zhang, X.; Ke, Y.; Wang, C.; Qui, Z.; Tang, Y. A Review on Silicon Nanowire Based Anodes for Next-Generation High-Performance Lithium-Ion Batteries from a Material-Based Perspective. *Sustain. Energy Fuels* **2020**, *4*, 1577–1594. [[CrossRef](#)]
8. Kato, S.; Kurokawa, Y.; Gotoh, K.; Soga, T. Silicon Nanowire Heterojunction Solar Cells with an Al₂O₃ Passivation Film Fabricated by Atomic Layer Deposition. *Nanoscale Res. Lett.* **2019**, *14*, 99. [[CrossRef](#)] [[PubMed](#)]
9. Yang, C.; Chandran, K.S.R. A Critical Review of Silicon Nanowire Electrodes and Their Energy Storage Capacities in Li-Ion Cells. *RSC Adv.* **2023**, *13*, 3947–3957. [[CrossRef](#)]
10. Farid, G.; Amade-Rovira, R.; Ma, Y.; Ospina, R.; Serafin, J.; Chaitoglou, S.; Majumdar, S.; Poveda, A.; Bertran-Serra, E. Improving Lithium-Ion Battery Performance through Patterned Growth of Carbon Nanotubes over Vertically Aligned Silicon Nanowires. *J. Energy Storage* **2024**, *101*, 113830. [[CrossRef](#)]
11. Coffinier, Y.; Boukherroub, R. Chapter 3. Surface Modification of Silicon Nanowires for Biosensing. In *Semiconducting Silicon Nanowires for Biomedical Applications*; Elsevier: Amsterdam, The Netherlands, 2022; pp. 25–68. [[CrossRef](#)]
12. Izuan, J.; Rashid, A.; Abdullah, J.; Yusof, N.A.; Hajian, R. The Development of Silicon Nanowire as Sensing Material and Its Applications. *J. Nanomater.* **2013**, *2013*, 328093. [[CrossRef](#)]
13. Keribi, M.; Nafie, N.; Boujmil, M.F.; Bouaicha, M. Response Modulation of Silicon Nanowires-Based Sensor to Carbon Number in Petroleum Vapor Detection. *Fuel* **2021**, *304*, 121260. [[CrossRef](#)]
14. Ahoulou, S.; Perret, E.; Nedelec, J.-M. Functionalization and Characterization of Silicon Nanowires for Sensing Applications: A Review. *Nanomaterials* **2021**, *11*, 999. [[CrossRef](#)]
15. Aradi, B.; Ramos, L.E.; Deák, P.; Köhler, T.; Bechstedt, F.; Zhang, R.Q.; Frauenheim, T. Theoretical Study of the Chemical Gap Tuning in Silicon Nanowires. *Phys. Rev. B* **2007**, *76*, 035305. [[CrossRef](#)]
16. Schmidt, V.; Wittemann, J.V.; Senz, S.; Gösele, U. Silicon Nanowires: A Review on Aspects of Their Growth and Their Electrical Properties. *Adv. Mater.* **2009**, *21*, 2681–2702. [[CrossRef](#)]
17. Priolo, F.; Gregorkiewicz, T.; Galli, M.; Krauss, T.F. Silicon Nanostructures for Photonics and Photovoltaics. *Nat. Nanotechnol.* **2014**, *9*, 19–32. [[CrossRef](#)]
18. Ninno, D.; Iadonisi, G.; Buonocore, F. Carrier Localization and Photoluminescence in Porous Silicon. *Solid State Commun.* **1999**, *112*, 521–525. [[CrossRef](#)]
19. Bashouti, M.Y.; Stelzner, T.; Berger, A.; Christiansen, S.; Haick, H. Chemical Passivation of Silicon Nanowires with C₁–C₆ Alkyl Chains through Covalent Si–C Bonds. *J. Phys. Chem. C* **2008**, *112*, 19168–19172. [[CrossRef](#)]
20. Banerjee, D.; Benavides, J.A.; Guo, X.; Cloutier, S.G. Tailored Interfaces of the Bulk Silicon Nanowire/TiO₂ Heterojunction Promoting Enhanced Photovoltaic Performances. *ACS Omega* **2018**, *3*, 5064–5070. [[CrossRef](#)]
21. Bashouti, M.Y.; Sardashti, K.; Schmitt, S.W.; Pietsch, M.; Ristein, J.; Haick, H.; Christiansen, S.H. Oxide-Free Hybrid Silicon Nanowires: From Fundamentals to Applied Nanotechnology. *Prog. Surf. Sci.* **2013**, *88*, 39–60. [[CrossRef](#)]
22. Veerbeek, J.; Huskens, J. Applications of Monolayer-Functionalized H-Terminated Silicon Surfaces: A Review. *Small Methods* **2017**, *1*, 1700072. [[CrossRef](#)]
23. Bashouti, M.Y.; Stelzner, T.; Christiansen, S.; Haick, H. Covalent Attachment of Alkyl Functionality to 50 Nm Silicon Nanowires through a Chlorination/Alkylation Process. *J. Phys. Chem. C* **2009**, *113*, 14823–14828. [[CrossRef](#)]
24. Abu Much, R.; Natarajan, P.; Shalabny, A.; Sadhujan, S.; Harilal, S.; Y. Bashouti, M. Heterojunction-Based Hybrid Silicon Nanowires Solar Cell. In *Solar Cells*; Nayeripour, M., Mansouri, M., Waffenschmidt, E., Eds.; IntechOpen: Rijeka, Croatia, 2020; ISBN 978-1-78984-125-1.
25. Akbari-Saatlu, M.; Procek, M.; Mattsson, C.; Thungström, G.; Nilsson, H.-E.; Xiong, W.; Xu, B.; Li, Y.; Radamson, H.H. Silicon Nanowires for Gas Sensing: A Review. *Nanomaterials* **2020**, *10*, 2215. [[CrossRef](#)]
26. Ng, M.-F.; Sim, L.Y.; Da, H.; Jin, H.; Lim, K.H.; Yang, S.-W. Modulation of the Work Function of Silicon Nanowire by Chemical Surface Passivation: A DFT Study. *Theor. Chem. Acc.* **2010**, *127*, 689–695. [[CrossRef](#)]
27. Ma, D.; Chen, J.; Li, J.; Ji, X.; Shi, J.-W. A Review on Passivation Engineering for Improving Photocatalytic Hydrogen Evolution Performance. *J. Mater. Chem. A* **2024**, *12*, 12293–12324. [[CrossRef](#)]
28. Natan, A.; Kroni, L.; Haick, H.; Tung, R.T. Electrostatic Properties of Ideal and Non-Ideal Polar Organic Monolayers: Implications for Electronic Devices. *Adv. Mater.* **2007**, *19*, 4103–4117. [[CrossRef](#)]

29. Bashouti, M.Y.; Tung, R.T.; Haick, H. Tuning the Electrical Properties of Si Nanowire Field-Effect Transistors by Molecular Engineering. *Small* **2009**, *5*, 2761–2769. [[CrossRef](#)] [[PubMed](#)]
30. Yoshitake, M. *Work Function and Band Alignment of Electrode Materials: The Art of Interface Potential for Electronic Devices, Solar 452 Cells, and Batteries (NIMS Monographs)*, 1st ed.; (English Edition); Springer: Berlin/Heidelberg, Germany, 2021; pp. 97–112.
31. Njema, G.G.; Kibet, J.K.; Ngari, S.M. A Review of Interface Engineering Characteristics for High Performance Perovskite Solar Cells. *Meas. Energy* **2024**, *2*, 100005. [[CrossRef](#)]
32. Yu, X.; Shen, X.; Mu, X.; Zhang, J.; Sun, B.; Zeng, L.; Yang, L.; Wu, Y.; He, H.; Yang, D. High Efficiency Organic/Silicon-Nanowire Hybrid Solar Cells: Significance of Strong Inversion Layer. *Sci. Rep.* **2015**, *5*, 17371. [[CrossRef](#)] [[PubMed](#)]
33. Raman, S.; Ravi, S.A.; Sindhuja, M. Advances in Silicon Nanowire Applications in Energy Generation, Storage, Sensing, and Electronics: A Review. *Nanotechnology* **2023**, *34*, 182001. [[CrossRef](#)] [[PubMed](#)]
34. Buonocore, F.; Marchio, S.; Giusepponi, S.; Celino, M. Computational Insights into the Energetics of Single C2–C10 Aliphatic Moieties Adsorbed on the Hydrogenated Silicon (111) Surface. *Langmuir* **2025**, *41*, 9706–9715. [[CrossRef](#)]
35. Ferrucci, B.; Buonocore, F.; Giusepponi, S.; Shalabny, A.; Bashouti, M.Y.; Celino, M. Ab Initio Study of Octane Moiety Adsorption on H- and Cl-Functionalized Silicon Nanowires. *Nanomaterials* **2022**, *12*, 1590. [[CrossRef](#)]
36. Hohenberg, P.; Kohn, W. Inhomogeneous Electron Gas. *Inhomogeneous Electron Gas* **1964**, *136*, B864–B871. [[CrossRef](#)]
37. Kohn, W.; Sham, L.J. Self-Consistent Equations Including Exchange and Correlation Effects. *Phys. Rev.* **1965**, *140*, A1133–A1138. [[CrossRef](#)]
38. Giannozzi, P.; Baroni, S.; Bonini, N.; Calandra, M.; Car, R.; Cavazzoni, C.; Ceresoli, D.; Chiarotti, G.L.; Cococcioni, M.; Dabo, I.; et al. QUANTUM ESPRESSO: A Modular and Open-Source Software Project for Quantum Simulations of Materials. *J. Phys. Condens. Matter* **2009**, *21*, 395502. [[CrossRef](#)]
39. Giannozzi, P.; Andreussi, O.; Brumme, T.; Bunau, O.; Buongiorno Nardelli, M.; Calandra, M.; Car, R.; Cavazzoni, C.; Ceresoli, D.; Cococcioni, M.; et al. Advanced Capabilities for Materials Modelling with Quantum ESPRESSO. *J. Phys. Condens. Matter* **2017**, *29*, 465901. [[CrossRef](#)] [[PubMed](#)]
40. Perdew, J.P.; Burke, K.; Ernzerhof, M. Generalized Gradient Approximation Made Simple. *Phys. Rev. Lett.* **1996**, *77*, 3865–3868. [[CrossRef](#)] [[PubMed](#)]
41. Vanderbilt, D. Soft Self-Consistent Pseudopotentials in a Generalized Eigenvalue Formalism. *Phys. Rev. B Condens. Matter* **1990**, *41*, 7892–7895. [[CrossRef](#)]
42. Monkhorst, H.J.; Pack, J.D. Special Points for Brillouin-Zone Integrations. *Phys. Rev.* **1976**, *13*, 5188–5192. [[CrossRef](#)]
43. Grimme, S.; Antony, J.; Ehrlich, S.; Elge Krieg, H. A Consistent and Accurate Ab Initio Parametrization of Density Functional Dispersion Correction (DFT-D) for the 94 Elements H–Pu. *Chem. Phys.* **2010**, *132*, 154104–154119. [[CrossRef](#)]
44. Buonocore, F.; Lisi, N.; Pulci, O. Electronic and Optical Properties of Metal Decorated Nitrogen-Doped Vacancy Defects in Graphene. *J. Phys. Condens. Matter* **2019**, *31*, 235302. [[CrossRef](#)] [[PubMed](#)]
45. Marchio, S.; Buonocore, F.; Giusepponi, S.; Celino, M. Density Functional Theory Study of Silicon Nanowires Functionalized by Grafting Organic Molecules. *Mater. Cloud Arch.* **2025**, *101*. [[CrossRef](#)]
46. Rino, J.P.; Ebbsjö, I.; Branicio, P.S.; Kalia, R.K.; Nakano, A.; Shimojo, F.; Vashishta, P. Short- and Intermediate-Range Structural Correlations in Amorphous Silicon Carbide: A Molecular Dynamics Study. *Phys. Rev. B* **2004**, *70*, 045207. [[CrossRef](#)]
47. Fox, M.A.; Whitesell, J.K. *Organic Chemistry*; Jones & Bartlett Learning: Sudbury, MA, USA, 2004.
48. Haziri, V.; Phal, S.; Boily, J.-F.; Berisha, A.; Tesfalidet, S. Oxygen Interactions with Covalently Grafted 2D Nanometric Carboxyphenyl Thin Films—An Experimental and DFT Study. *Coatings* **2022**, *12*, 49. [[CrossRef](#)]
49. Jing, Z.; Whitten, J.L. Ab Initio Studies of H Chemisorption on Si(100) Surface. *Phys. Rev. B* **1992**, *46*, 9544. [[CrossRef](#)]
50. Bruno, M.; Palumbo, M.; Marini, A.; Del Sole, R.; Ossicini, S. From Si Nanowires to Porous Silicon: The Role of Excitonic Effects. *Phys. Rev. Lett.* **2007**, *98*, 036807. [[CrossRef](#)] [[PubMed](#)]
51. Wang, X.; Dvorak, M.; Wu, Z. Hybrid Functionals with Fixed Mixing Parameter Perform No Better than PBE for Fundamental Band Gaps of Nanoscale Materials. *Phys. Rev. B* **2016**, *94*, 195429. [[CrossRef](#)]
52. Capelle, K. A Bird’s-Eye View of Density-Functional Theory. *Braz. J. Phys.* **2006**, *36*, 1318–1343. [[CrossRef](#)]
53. Bhattacharjee, S.; Koshi, N.A.; Lee, S.-C. Customizing PBE Exchange-Correlation Functionals: A Comprehensive Approach for Band Gap Prediction in Diverse Semiconductors. *Phys. Chem. Chem. Phys.* **2024**, *26*, 26443–26452. [[CrossRef](#)]
54. Lejaeghere, K.; Bihlmayer, G.; Björkman, T.; Blaha, P.; Blügel, S.; Blum, V.; Caliste, D.; Castelli, I.E.; Clark, S.J.; Dal Corso, A.; et al. Reproducibility in Density Functional Theory Calculations of Solids. *Science* **2016**, *351*, aad3000. [[CrossRef](#)] [[PubMed](#)]
55. Bashouti, M.Y.; Garzuzi, C.A.; De La Mata, M.; Arbiol, J.; Ristein, J.; Haick, H.; Christiansen, S. Role of Silicon Nanowire Diameter for Alkyl (Chain Lengths C₁–C₁₈) Passivation Efficiency through Si–C Bonds. *Langmuir* **2015**, *31*, 2430–2437. [[CrossRef](#)] [[PubMed](#)]
56. Rogozhina, E.V.; Eckhoff, D.A.; Gratton, E.; Braun, P.V. Carboxyl Functionalization of Ultrasmall Luminescent Silicon Nanoparticles through Thermal Hydrosilylation. *J. Mater. Chem.* **2006**, *16*, 1421. [[CrossRef](#)]
57. Molteni, E.; Cappellini, G.; Cardia, R.; Onida, G.; Mula, G. Eumelanin Adsorption on Silicon: Optical Properties of Si(001)-Adsorbed Eumelanin Tetrameric Protomolecules. *J. Phys. Chem. C* **2020**, *124*, 9376–9384. [[CrossRef](#)]

58. He, L.; Jiang, C.; Wang, H.; Lai, D. Si Nanowires Organic Semiconductor Hybrid Heterojunction Solar Cells Toward 10% Efficiency. *ACS Appl. Mater. Interfaces* **2012**, *4*, 1704–1708. [[CrossRef](#)]
59. Shen, X.; Ma, B.; Chen, L.; Zhao, J. High Efficiency Conjugated Polymer/Si Hybrid Solar Cells with Tetramethylammonium Hydroxide Treatment. *RSC Adv.* **2017**, *7*, 688–693. [[CrossRef](#)]
60. Cullis, A.G.; Canham, L.T.; Calcott, P.D.J. The Structural and Luminescence Properties of Porous Silicon. *J. Appl. Phys.* **1997**, *82*, 909–965. [[CrossRef](#)]
61. Iannone, F.; Ambrosino, F.; Bracco, G.; De Rosa, M.; Funel, A.; Guarnieri, G.; Migliori, S.; Palombi, F.; Ponti, G.; Santomauro, G.; et al. CRESCO ENEA HPC Clusters: A Working Example of a Multifabric GPFS Spectrum Scale Layout. In Proceedings of the 2019 International Conference on High Performance Computing & Simulation (HPCS), Dublin, Ireland, 15–19 July 2019; pp. 1051–1052.
62. Mariano, A.; D’Amato, G.; Ambrosino, F.; Aprea, G.; Buonocore, F.; Celino, M.; Colavincenzo, A.; Fina, M.; Funel, A.; Giusepponi, S.; et al. Fast Access to Remote Objects 2.0 a Renewed Gateway to ENEAGRID Distributed Computing Resources. *Future Gener. Comput. Syst.* **2019**, *94*, 920–928. [[CrossRef](#)]

Disclaimer/Publisher’s Note: The statements, opinions and data contained in all publications are solely those of the individual author(s) and contributor(s) and not of MDPI and/or the editor(s). MDPI and/or the editor(s) disclaim responsibility for any injury to people or property resulting from any ideas, methods, instructions or products referred to in the content.